Journal of Applied Polymer Science

New Approach for Preparation of Exfoliated Clay Hybrid via Wet Kneading Masterbatch Process

Chi-Yuan Hung,[1] Cheng-Chien Wang,[2] Chuh-Yung Chen[1,3]

[1]Department of Chemical Engineering, National Cheng Kung University, 70101, Tainan, Taiwan
[2]Department of Chemical and Materials Engineering, Southern Taiwan University of Science and Technology, 71005, Tainan, Taiwan
[3]Research Center for Energy Technology and Strategy, National Cheng Kung University, 70101 Tainan, Taiwan
Correspondence to: C.-Y. Chen (E-mail: ccy7@ccmail.ncku.edu.tw)

ABSTRACT: Through using modified masterbatch method which comprised the wet kneading and intercalated modifiers process, the fully exfoliated nylon clay hybrids (NCHs) were achieved. In the wet kneading procedure, the organoclay plates were easily wetting by the intercalated modifiers. Then the shearing force could completely exfoliate the organoclay with nylon 6 matrix even which only had lower molecular weight during the extrusion process. NCEs and NCAs, two series of NCHs, were prepared from the intercalated modifiers, alkylamide and polyamide, respectively. The XRD and TEM examinations show that the fully exfoliated NCHs can easily be made. The NCEs show a faster crystallization rate because alkylamide with the lower molecular length and the melting temperature act as a soft segment to make crystallization more easily and more regularly. The tensile test shows that the NCEs have higher values of modulus and yield strength and the NCAs can keep better elongation properties. Furthermore, the tensile specimen shows a cone-like fracture, which is considered more perfectly exfoliated and arranged because of the good interaction between the silicate plates and nylon 6. © 2012 Wiley Periodicals, Inc. J. Appl. Polym. Sci. 000: 000–000, 2012

KEYWORDS: clay; extrusion; polyamides

Received 29 March 2012; accepted 4 August 2012; published online
DOI: 10.1002/app.38436

INTRODUCTION

Since the detailed investigation of Toyota researchers on polymer layered silicate clay mineral composites, the nylon 6 containing exfoliated organoclay nanocomposites became one of the most important hybrid nanocomposites because they showed remarkable improvements in certain physic-mechanical properties.[1,2] These nanocomposites offer exceptional stiffness and strength at very low filler loading, whereas three times this amount of glass fibers is needed to achieve the same improvements.[3] The organoclay nanocomposites also exhibit unexpected synergistically enhanced hybrid properties such as elasticity modulus, strength,[4,5] thermal resistance, heat distortion temperature,[6,7] flame retardant capability,[8,9] and gas barrier.[10,11] Thus, the nanocomposites have been a popular investigation topic in academic, industrial, and governmental studies.

To prepare nylon clay hybrids (NCHs), three major methods were developed: in-situ polymerization method, compounding method, and solution method. In-situ polymerization method was first disclosed, wherein caprolactam was polymerized in the presence of organophilic montmorillonite ion-exchanged with ammonium ions of aminoacid.[1] Unfortunately, the cost of in-situ polymerization method is too high, and it is not suitable for polymer compounding. In the solution methods, which used mild preparation conditions, the clay platelets restacked after the solvent evaporated. The disadvantages of solution method are air-pollution caused in the solvent elimination process and it is also not suitable for polymer compounding factory. Industrially, the melt compounding processes have attracted a great deal of attention. For example, Vaia et al. presented the direct polymer melt intercalation method to prepare nanocomposites, where polymer chains were diffused into the space between the clay layers.[12,13] Qi et al. studied the blending of nylon 6 and the organoclay, which was ion-exchanged by organoammonium ions with melt compounded processes.[14] He found that the organoclay was necessary in the formation of the exfoliated-type NCHs because the silicate layers with organo-modification had a better interaction with the polymers and produced the exfoliated nanocomposites during compounding. Furthermore, Paul et al. investigated the NCHs in their processing method, dispersed modeling, morphology, and thermal and mechanical properties[15–21] and suggested that this approach could be combined with the conventional polymer processing techniques such as extrusion to decrease the time to form these

Table I. The Recipe and Sample ID for the Preparation of NCHs

	Sample ID								
Composition	NY6	NC1	NCE1	NCE3	NCE5	NCA1	NCA3	NCA5	NCA10
Organoclay (wt %)	0	1	1	3	5	1	3	5	10
Modifier type	–	–	alkylamide	alkylamide	alkylamide	polyamide	polyamide	polyamide	polyamide
Modifier (wt %)	–	–	0.5	1.5	2.5	1	3	5	10
Nylon 6 (wt %)	100	99	98.5	95.5	92.5	98	94	90	80

well-exfoliated hybrids. They also pointed out that the higher molecular weight grades of nylon 6 led to higher levels of exfoliation of NCHs. In order to improve the melt process to achieve good exfoliation in all molecular weight grades of NCHs, researches tried to modify the process with other procedures such as the masterbatch methods[22] and the slurry methods.[23] However, the slurry methods need additional equipment installations, causing the processing facility costs to rise. On the other hand, the NCHs made by the masterbatch methods have some local silicate layers aggregated. Hence, how to overcome the aggregation of silicate layers in the masterbatch methods using low molecular weight grades of nylon 6 has become an interested topic in the NCH industry.

To get well-exfoliated NCHs, the organoclays with higher basal spacing were usually obtained from introducing alkylammonium cations into the clay interlayer.[18,21,24] Those studies also pointed out that the longer alkylammonium cations not only led higher basal spacing of clay interlayer but also made the silicate surface more hydrophobic with the long chain hydrocarbons. The more hydrophobic silicate surfaces led poor exfoliation in the polar polymer matrix, such as nylon. In the early period, Usuki et al. found out that using the ammonium cations of ω-amino acid as the interlayer cations obtained the NCHs in the in-situ polymerization.[1,25] They also indicated that amino acid could provide good chemical attraction with the amide group of ε-caprolactam.

Through this concept, we used the kneading machine with wetting milling to swell the organoclay contained ammonium cations of ω-amino acid and introduce the intercalated modifiers within the amide group, which provided a strong hydrogen bonding between nylon 6 and the organoclay to form the organoclay masterbatches. Two different molecular weight amide compounds were used as intercalated modifiers: alkylamide, which has a lower molecular weight (ca. 500 Da), aliphatic polyamide, which has a higher molecular weight (ca. 1500∼3000 Da) and was less crystalline. Through this wet kneading procedure, the organoclay plates were easily wetting by the intercalated modifiers. Due to the well wetting and strong hydrogen bonding, the well-exfoliated nanocomposites were obtained by melt blending the masterbatches with the low molecular weight nylon 6. The characterizations and the properties of the NCHs made from the masterbatches were examined using XRD, TEM, DSC, tensile test, and WVPR. In addition, these data were compared with those of equivalent nanocomposites prepared by the direct melt processing method.

EXPERIMENT

Materials

Nylon 6 (NY6) is a commercially available material from DSM: Akulon F223D with low viscosity. The number average molecular weight is about 16,900 Da, determined via the intrinsic viscosity using m-cresol at 25°C and calculated from the expression: $[\eta] = 5.26 \times 10^{-4}\overline{M_w}^{0.745}$, assuming $\overline{M_n} = 1/2\overline{M_w}$.[15] The organoclay which was exchanged with ammonium cations of ω-amino acid was purchased from Nanocor under the trade name Nanomer®I.24TL. The two kinds of intercalated modifiers, alkylamide (a derivatives of stearamide, PL-101, $M_w \sim 500$ Da, $T_m \sim 145$°C) and aliphatic polyamide (Sunmide 550, M_w: 1500–3000 Da) were kindly donated by GWIP, Taiwan.

Melt Processing

A two-step process was used to prepare the nanocomposites with the desired organoclay content. In the first step, the organoclay slurry, which was prepared by dispersing organoclay into ethanol (3000 g, 20 wt %) in 48 h to swell the silicate interlayer, was slowly added into the intercalated modifier solution (1800 g, 33 wt % in toluene) and kneaded (Irie Shokai, PNV-5 H kneader, set at 45 rpm) at 90°C for 3 h to evaporate the solvent. Through this wet kneading process, it provided higher shear force to make the swollen organoclay intercalated. The amide modifier could intercalate into the silicate interlayer and have strong attraction with amino acid. Then, it was further dried in a vacuum oven at 80°C for 24 h to obtain the organoclay masterbatches. The recipe of the organoclay and the modifiers is shown in Table I. In the second step, the nylon 6 nanocomposites containing 1, 3, and 5 wt % organoclay were prepared by melt blending the organoclay masterbatches and nylon 6 in a Werner and Pfleiderer corotating, twin screw-extruder (Model-ZSK 26 MEGA compounder, diameter = 26 mm, L/D = 56). The barrel temperature was set at 220°C; the screw speed and the feed-rate were set at 500 rpm and 800 g/h, respectively. Prior to the extrusion, all nylon 6 nanocomposites were dried in a vacuum oven at 80°C for 16 h. For comparison, the nylon 6 nanocomposites without the intercalated modifier were also prepared using the same organoclay and processing conditions mentioned above. Based on the recipes, the nylon clay hybrids were defined as NCXY, where X represents the types of intercalated modifier, E for alkylamide modifier and A for polyamide modifier, and Y represents the weight percentage of organoclay in the hybrids. The detail recipe of the prepared nanocomposites is given in Table I.

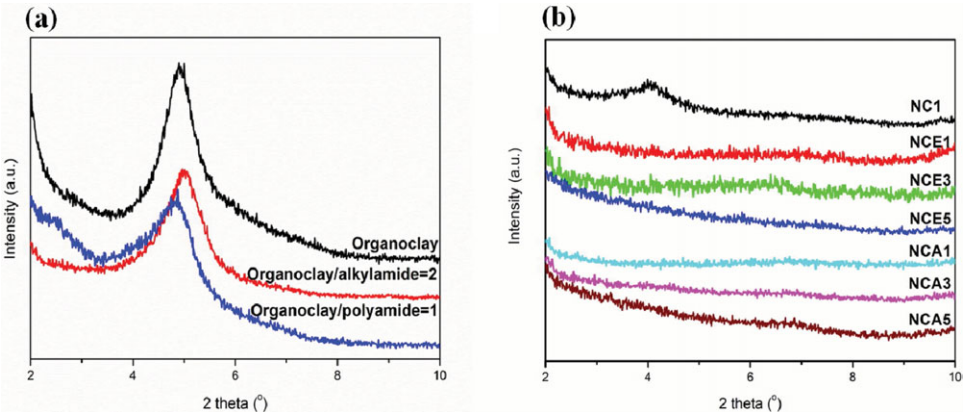

Figure 1. XRD patterns for (a) organoclay and its masterbatches (b) NCHs. [Color figure can be viewed in the online issue, which is available at wileyonlinelibrary.com.]

Characterization

The XRD measurements were used to identify the distance of the silicate organoclay layer. All experiments were performed using a Rigaku Rint 2000 unit with Cu Kα radiation at a voltage of 40 kV and a current of 40 mA. The scans were taken from 2θ = 2°–30° with the scan speed 1.0°/min and the scan step 0.02°.

Fourier transfer infrared (FTIR) spectra were recorded with a Varian 2000 FTIR analyzer, which operated from 700 to 4000 cm^{-1} at room temperature. Spectra were obtained using a resolution of 4 cm^{-1} and were averaged over 64 scans. The samples were mixed thoroughly with potassium bromide (KBr) at ~3 wt %, and the resulting powders were pressed into a transparent pellet.

The TEM micrographs of the nanocomposites were obtained using a Hitachi H-7500 with an acceleration voltage of 80 kV. The specimens were prepared using an ultrathin microtome. Thin cross sections with a thickness of ~60 nm were cut using a diamond knife at 30°C. The cutting directions were parallel to the extrusion direction.

Thermal characterization was performed in an atmosphere of dry nitrogen using DSC (TA Instruments Q2000). Both temperature and heat flow were calibrated using the indium and tin standards. In the DSC measurement, a polymer sample was preheated at 260°C for 5 min to remove its thermal history and memory effects, and then it was cooled to 30°C at a rate of 10°C/min. Next, the cooled sample was heated to 260°C at 10°C/min. T_m (melting temperature) and T_c (crystallization temperature) are the peak temperatures measured in the heating run and the cooling run, respectively.

The tensile (ASTM D638) and notched impact (ASTM D256) specimens were prepared by injection molding, using an FCS FT-100 injection molding machine with a barrel temperature of 260°C, a mold temperature of 80°C, an injection pressure of 80 bar and a holding pressure of 40 bar. The universal tensile machine (Instron 4467) was then used to test the stress–strain properties at a constant crosshead speed of 20 mm/min. The fracture surfaces of the tensile specimens were also analyzed with an emission scanning electron microscope (SEM) (JEOL JSM-6390LA). Izod impact specimens were notched (45° V-notch) to a depth of 2.54 mm on one side of the bar. All tests were performed at ambient temperature (25°C) and at least five samples of each composition were tested and the average values reported.

The water vapor barrier testing was carried out in accordance with the ASTM Standards F1249-06. The water vapor transmission was measured using a Modern Controls Inc. (MOCON) Permatran-W Model 3/61 and a humidified nitrogen flow rate of 100 SCCM at 100% RH and 23°C. The samples were carried out on sheets prior to the measurements with average thickness ~0.5 mm.

RESULTS AND DISCUSSIONS

To improve the melting process to achieve good exfoliation in low molecular weight grades of nylon 6, the modified masterbatch methods with the wet kneading and the intercalated modifier process were used in this study. In the modified masterbatch methods, the organoclay slurry was dispersed in ethanol to swell the silicate interlayer. Then the intercalated modifier solution was slowly added and kneaded. Through this wet kneading process, it provided higher shear force to make the amide modifiers could intercalate into the silicate interlayer of the swollen organoclay. In addition, the amide modifier provided the well wetting and strong hydrogen bonding between nylon 6 and the organoclay in the NCHs. The intercalated modifier not only had strong attraction with organoclay but also acted as lubricant during the melting process.

Figure 1(a) shows the XRD patterns of the organoclay and the masterbatch powders made with the two modifiers. The organoclay pattern reveals a broad intense peak at around 2θ = 5°, corresponding to a basal spacing of 1.79 nm. The incorporation of polyamide into the organoclay could slightly increase the d-spacing (from 1.79 nm to 1.84 nm and 3.52 nm) while the alkylamide did not show the same result because its chain length is similar to that of the original modifier in the organoclay. Furthermore, the organoclay masterbatches and nylon 6 were melt blended in the twin screw extruder to obtain nylon

Applied Polymer SCIENCE

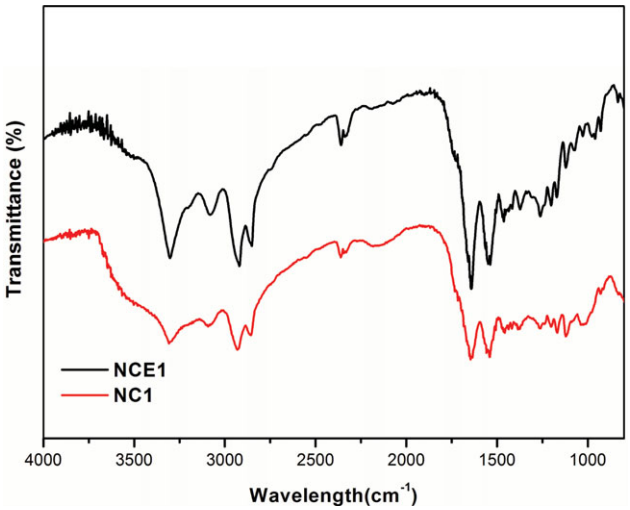

Figure 2. FTIR spectra of NCE1 and NC1. [Color figure can be viewed in the online issue, which is available at wileyonlinelibrary.com.]

6 nanocomposites. For comparison, the nylon 6 nanocomposites without the intercalated modifier, NC1, were also prepared using the same processing conditions. All of the nanocomposites were carried out on sheets prior to the XRD measurements. In Figure 1(b), the basal spacing of the organoclays disappears completely in the XRD patterns of all nanocomposites except the NC1 (ca. 2.2 nm). In order to confirm the intermolecular hydrogen bonding between the organoclay and nylon 6, the FT-IR spectra of NCE1 and NC1 was added in Figure 2. It shows the NCE1 provides the hydrogen bonding observed at about 1640 cm^{-1} (C = O), which is stronger than that in the composite without the modifier, NC1. Moreover, we also find the NCE1 has stronger hydrogen bonding of N-H at about 3304 cm^{-1} and less intensity of free amide vibration of N-H at about 3482 cm^{-1}. According to the result of FT-IR spectra, it shows incorporation of the intercalated modifiers into the amide group provides the hydrogen bonding between the organoclay and nylon 6. The absence of basal reflections in the XRD patterns for the NCE and NCA series of nanocomposites suggests that the polymer chains had penetrated into the galleries of layered silicates, delaminated them, and dispersed the individual silicate layers in the polymer matrices to form the fully exfoliated nanostructures.

The nanometer scale dispersions of the organoclays in the nylon 6 matrices were further corroborated with TEM images, as shown in Figure 3. The dark lines represent the intersection of the silicate layers, and the white background corresponds to the nylon 6 matrices. It shows bad exfoliated and a slight aggregation of silicate plates in NC1. The other TEM images of NCHs prepared by modified masterbatches process reveal that the organoclays are fully exfoliated in the nylon 6 matrices. Moreover, the TEM image of higher organoclay content, 10 wt %, NCHs named as NCA10 was also showed well exfoliated structure. Furthermore, the exfoliated clay platelets are parallel to the extrusion direction for all samples, and this effect can be attributed to the melt-flow-induced clay orientation during the melt blending process.[26,27] Hence, through this wet kneading masterbatch process, the fully exfoliated nanocomposites would be easily prepared by the melting process even with the higher organoclay content.

In addition, we observed the nonisothermal behavior using the heating and cooling scans for all specimens obtained from the extruder pellets. The DSC traces of the heating scans and the cooling scans, shown in Figure 4 reveal that the neat NY6 exhibits a rather broad melting peak (T_m) at around 222°C and

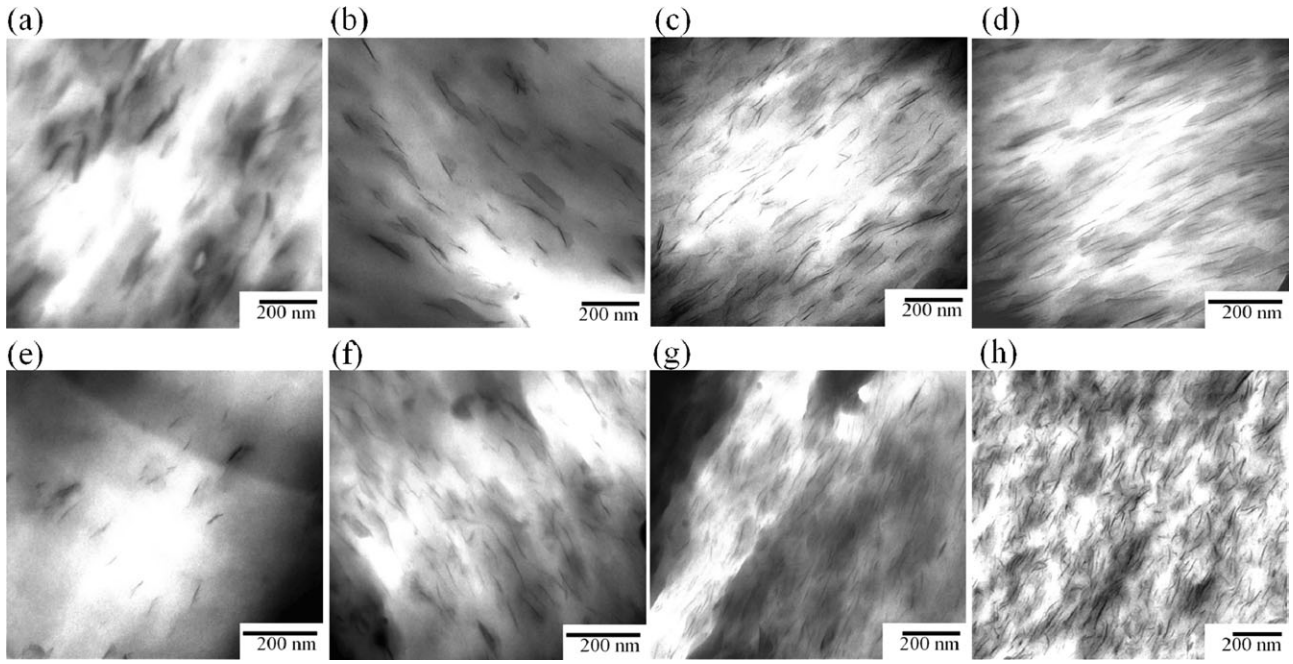

Figure 3. TEM micrographs of NCHs : (a) NC1, (b) NCE1, (c) NCE3, (d) NCE5, (e) NCA1, (f) NCA3, (g) NCA5, and (h) NCA10.

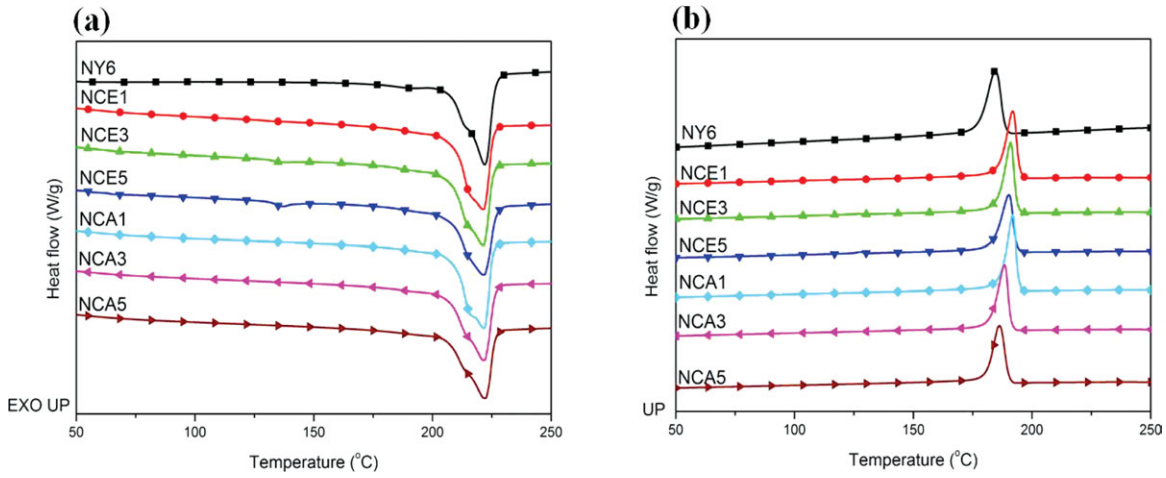

Figure 4. The DSC trace of NY6 and NCHs: (a) heating run, (b) cooling run. [Color figure can be viewed in the online issue, which is available at wileyonlinelibrary.com.]

a small shoulder at around 213°C, implying the presence of the α form as the major crystalline component. As the literature reported,[28–30] while adding clay into the NY6 matrix, the MMT platelet surface would induce more nucleation sites and facilitate the formation of γ-form crystals, polymorphic behavior. However, increasing the organoclay content does not cause a dramatic increase of the γ form regime or a disappearance of the α form regime in Figure 4(a). This phenomenon might be attributed to the amide modifiers which had interaction with the amino acid of the ammonium cation attached the MMT platelet surface to reduce the nucleating effect. Thus, the polymer chains of NY6 tethered to the MMT platelet surface are less constrained, and this leads to higher mobility of the polymer chains to form the α-form crystals. Furthermore, we noticed that the cooling scan curves showed a rapid crystallization of the nanocomposite, especially in the NCE series [Figure 4 (b)]. Because of the amide modifiers having a lower melting temperature and a regular structure, they can act as a soft segment with the flexibility to let the molecular chain crystallize more easily and more perfectly. However, the crystalline temperature would slightly decrease with the increasing of organoclay content because the silicate plate could hinder the crystalline growth of nylon 6. The shorter molecular length and the lower melting temperature of alkylamide could dramatically enhance the crystallization rate even in the higher organoclay content which the hinder effect was major concerned. All thermal properties of the nylon 6 nanocomposites were summarized in Table II. XRD was also used to evaluate the crystalline morphologies of the species (thickness∼0.2 mm), which went through thermal treatment at a cooling rate of 10 °C/min from the melted state. The pattern of NY6 shows two α form crystalline peaks at 20.2° and 24° and the γ form ones at 22.2°, as shown in Figure 5. In addition, the γ form ratios of NY6, NCE, NCA, and NC1 which were calculated by deconvoluted the XRD pattern were about 37%, 32%, 34%, and 40% respectively. It reveals the increase of γ form ratio in NC1 due to the nucleating effect of the MMT platelets. Furthermore, the NCHs prepared with amide group modifiers, NCE and NCA, show slight less γ form ratios than NY6. This result may be attributed to the amide group modifiers, which were attached with a silicate plate surface to reduce the nucleating effect of the MMT platelets, increase the interaction and provide flexibility that helped the nylon 6 molecule

Table II. The Thermo Properties of NY6 and NCHs

	First cooling		Second heating		
Sample	T_c (°C)	ΔH_c (J/g)	T_m[a] (°C)	ΔH_m (J/g)	χ_c[b] (%)
NY6	184.7	86.10	213.6/222.0	71.13	29.64
NCE1	191.9	82.01	215.4/221.3	77.15	32.64
NCE3	191.0	77.06	214.6/221.2	72.79	31.75
NCE5	190.3	72.39	214.5/221.5	66.55	29.98
NCA1	191.9	75.70	215.7/221.7	75.20	31.97
NCA3	188.5	69.48	213.9/221.5	71.88	29.95
NCA5	186.3	66.81	213.4/221.9	61.12	25.47

[a]Values in italics represent minor low temperature endotherms, [b]Crystallinity is calculated by the expression: $\chi_c(\%) = \frac{\Delta H_m}{(1-\varphi)\Delta H_m^\circ} \times 100$, where ΔH_m° is the average of $\Delta H_m^\circ(\alpha)$ and $\Delta H_m^\circ(\gamma)$ obtained from Ref. [15], i.e., 240 J/g, and φ is the weight fraction of organoclay in the NCHs.

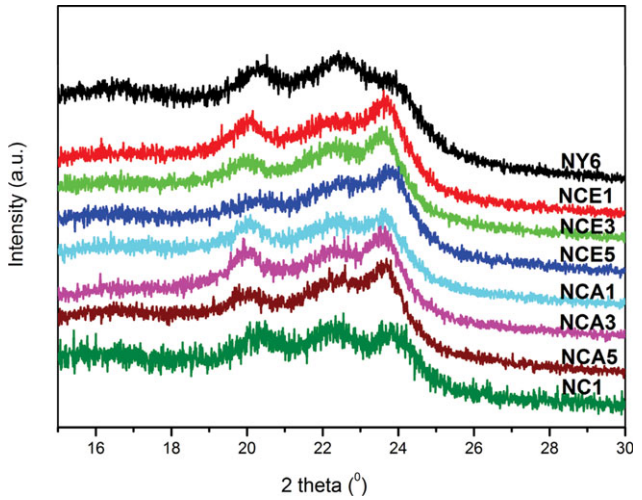

Figure 5. XRD diffraction pattern of NY6 and NCHs after heating treatment. [Color figure can be viewed in the online issue, which is available at wileyonlinelibrary.com.]

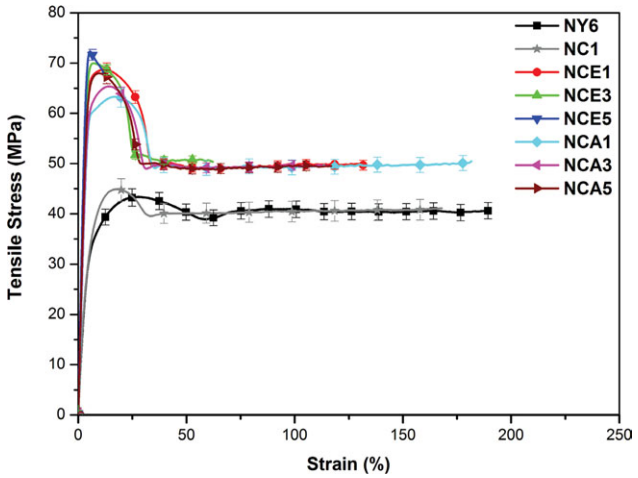

Figure 6. Stress–strain curves of NY6 and NCHs. [Color figure can be viewed in the online issue, which is available at wileyonlinelibrary.com.]

form the perfect α form crystal pattern. In other words, the crystallization behaviors of nylon 6 are strongly influenced by different intercalated modifiers of the masterbatches. We will investigate these behaviors in details and discuss them in our future studies.

The typical stress-strain curves and their tensile properties of nylon 6 and NCHs were shown and summarized in Figure 6 and Table III, respectively. Compared with the neat NY6, the NCH sample without the masterbatch processing sample, NC1, shows a slight increase of yield strength and a similar Young's modulus. However, NCE1 and NCA1 show dramatic enhancement of the Young's modulus and the yield strength compared with NC1. In addition, the mechanical properties of the NCE and NCA series were improved with the increasing of the organoclay content. It was also noteworthy that the NCE series have a higher modulus and more yield strength than the NCA series. However, at the highest organoclay content, the NCE5 is brittle and without yielding and necking. In contrast, the NCA5 reveals a necking and elongating feature. The alkylamide in NCEs makes the nylon 6 recrystallize and rearrange more easily, enhancing the stiffness during the drawing procedure. Higher alkylamide content would make the specimen too brittle to yield. In addition, the NCA series exhibited more ductile and better elongation properties because of the less crystalline modifier polyamide. Although the NCA5 had the elongation of 116%, it could overcome the weakness of NCHs for the applications that needed the high strength and the ductility.

The different fracture types of NCHs nanocomposites are shown in Figure 7. The samples, NCE1, NCE3, NCA3, and NCA5, displayed a cone-like fracture because the modifiers oriented the nylon 6 matrices to form more regular structure during the drawing procedure. This result could be further proved by scanning electron microscope (SEM), as shown in Figures 8 and 9. The NY6 shows a relatively smooth fracture surface [Figures 8(a) and 9(a)]. The NC1, an intercalated nanocomposite, reveals a coarser fracture pattern at both lower and higher magnifications [Figures 8(b) and 9(b)]. Obviously, the low interaction between the organoclay and nylon 6 inside NC1 would not make the organoclay slides parallel to the drawn direction and form the extensive plastic stretch of the matrix of nylon 6. However, the NCHs nanocomposites show an ordering topographic structure, as displayed in Figure 9. As mentioned above, the silicate platelets are parallel the specimen because of the melt-flow-induced orientation during the injection process. The exfoliated silicate platelets act as stress concentrators and provide the strengthened effects to the tensile specimen, which

Table III. Mechanical Properties of NY6 and NCHs

Sample	Modulus (MPa)	Yield strength (MPa)	Break Strength (MPa)	Elongation at Break (%)	Impact Strength(KJ/m^2)
NY6	1128 ± 45	43.3 ± 1.73	40.60 ± 1.62	190 ± 7.6	8.66 ± 0.35
NC1	1138 ± 57	44.9 ± 2.25	41.07 ± 2.05	168 ± 8.4	4.98 ± 0.25
NCE1	1864 ± 37	68.7 ± 1.37	49.77 ± 1.00	132 ± 2.6	4.31 ± 0.09
NCE3	2002 ± 30	69.9 ± 1.05	61.26 ± 0.92	51 ± 0.8	3.56 ± 0.05
NCE5	2218 ± 33	72.3 ± 1.08	67.89 ± 1.02	12 ± 0.2	2.28 ± 0.03
NCA1	1556 ± 47	63.3 ± 1.90	50.46 ± 1.51	182 ± 5.5	5.75 ± 0.17
NCA3	1698 ± 34	65.3 ± 1.31	49.50 ± 0.99	117 ± 2.3	4.85 ± 0.10
NCA5	1833 ± 37	68.0 ± 1.36	49.50 ± 1.00	116 ± 2.4	3.86 ± 0.08

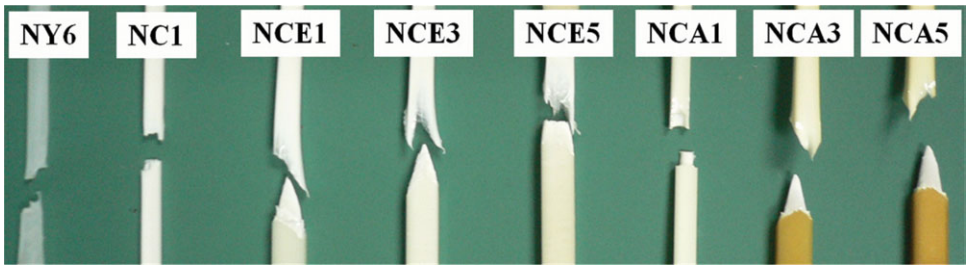

Figure 7. The fracture photographs of NY6 and NCHs after tensile test. [Color figure can be viewed in the online issue, which is available at wileyonlinelibrary.com.]

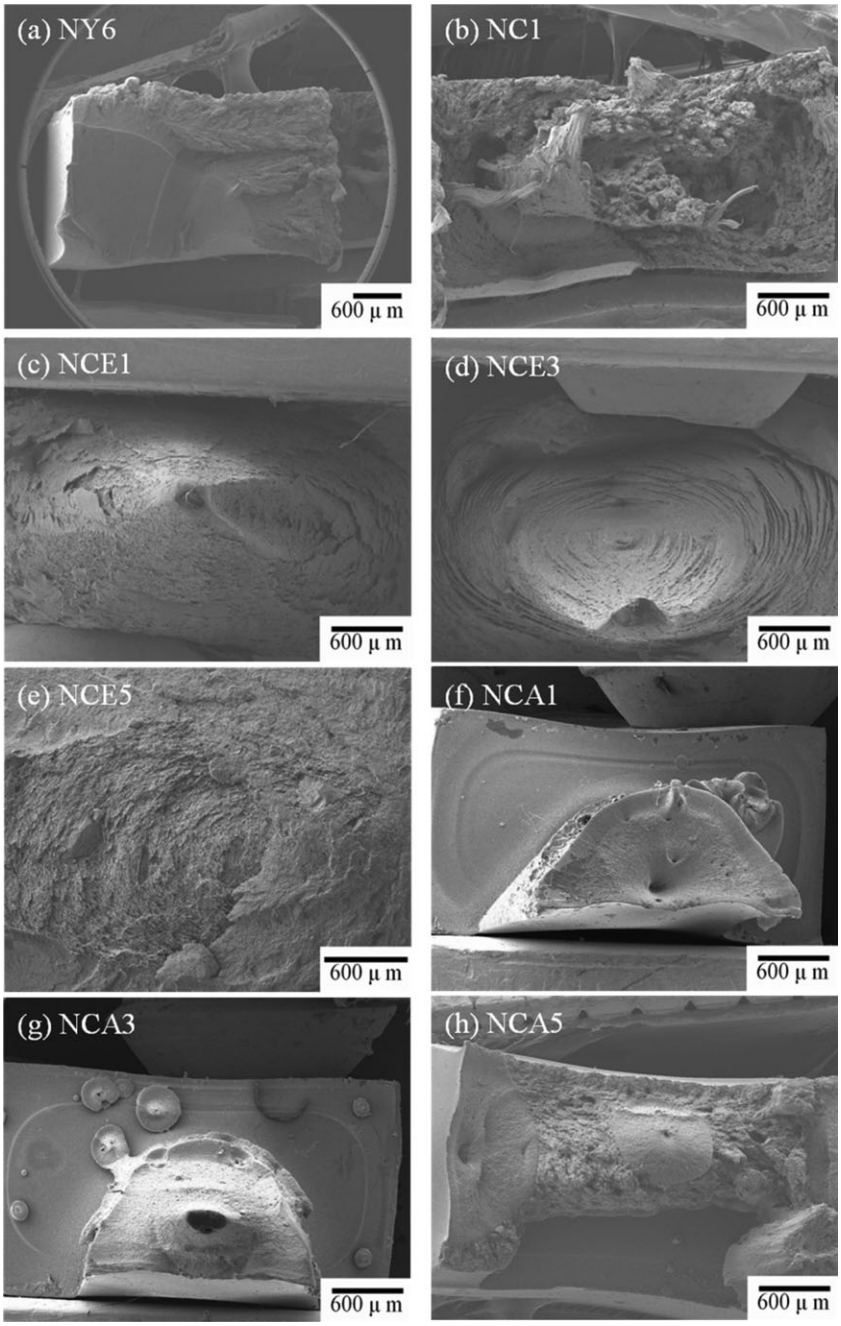

Figure 8. SEM micrographs of tensile fracture surfaces at low magnification: (a) NY6, (b) NC1, (c) NCE1, (d) NCE3, (e) NCE5, (f) NCA1, (g) NCA3, and (h) NCA5.

Applied Polymer SCIENCE

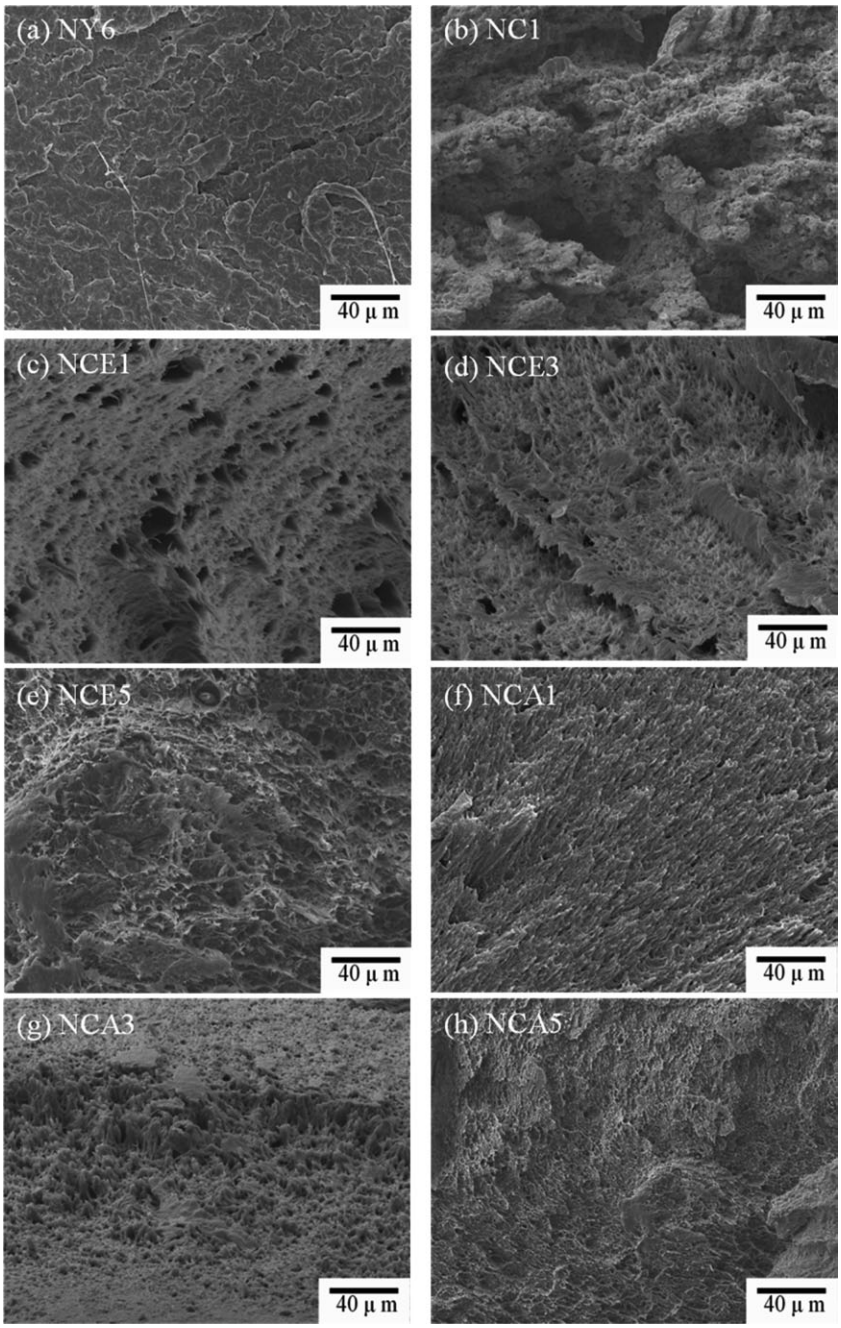

Figure 9. SEM micrographs of the tensile fracture surfaces at high magnification: (a) NY6, (b) NC1, (c) NCE1, (d) NCE3, (e) NCE5, (f) NCA1, (g) NCA3, and (h) NCA5.

causes the formation of multi-microvoids and directly favors the plastic fibrillation growing in the direction of drawing.[31] Notably, the specimen showed the cone-like photographs (Figure 7) instead of the obvious sheet-like or cabbage-like-sheets found in previous literature reports.[32,33] Because of the modifiers with the amide group, which allowed the formation of more hydrogen bonding between nylon 6 and silicate plates, the interaction bonding would strongly orient the silicate plates to surround the center of the specimen to form the smoother cone-like fracture during the drawing process. The NCE5 and NCA1 also show a fully exfoliated texture in the TEM micrographic; however, the cone-like fractures were not observed in the photographs and the SEM because the NCE5 with higher organoclay content was too brittle to form the multi-voiding and it oriented within the specimen before it broke. In contrast, the NCA series had more flexibility because of the amorphous polyamide. Thus, the lower organoclay content specimen, NCA1, was not able to orient to form a cone-like fracture because of the flexibility of the polyamide and the less silicate platelets. Consequently, the perfect cone-like fracture of NCHs was only appeared in NCE1, NCE3, NCA3, and NCA5.

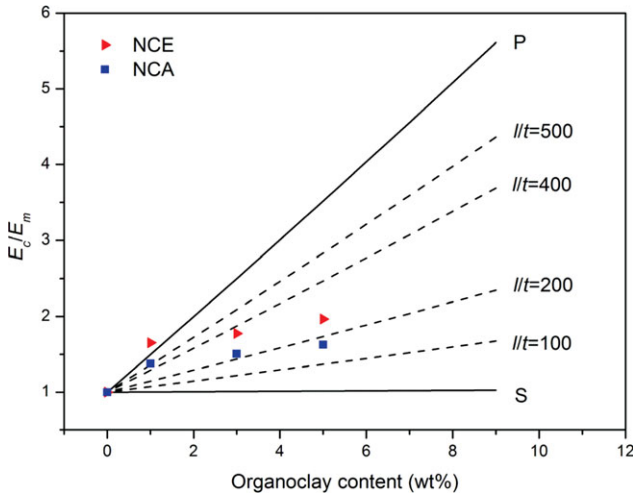

Figure 10. Effect on the organoclay content and the aspect (l/t) ratio on the modulus of NCHs. Using a value of $E_f = 200$ GPa, the solid lines P and S were calculated using eqs. (3) and (4), respectively. Similarly, the dashed line are Halpin-Tsai calculated using eqs. (1) for values of aspect ratio between 100 and 500. [Color figure can be viewed in the online issue, which is available at wileyonlinelibrary.com.]

Figure 10 shows the organoclay content and the aspect ratio on the modulus of the NCHs. The dash lines in Figure 10 were calculated using various aspect ratios between 100 and 500, according to the Halpin-Tsai model, which is a well-known composite theory to predict the stiffness of unidirectional composites as follows:

$$\frac{E_c}{E_m} = \frac{1 + \zeta\eta\varphi_f}{1 - \eta\varphi_f} \tag{1}$$

with

$$\eta = \frac{\frac{E_f}{E_m} - 1}{\frac{E_f}{E_m} + \zeta} \tag{2}$$

where E_c, E_f, and E_m are the composite, the reinforcement and the matrix Young's modulus; φ is the volume fraction of the filler and ζ is a shape factor dependent on the filler geometry and the loading direction. In this study, the value of ζ was taken as twice the aspect ratio of the reinforcing particles, i.e., $\zeta = 2(l/t)$, where l and t are the length and the thickness of the silicate plate. As $\zeta \to \infty$, eq. (1) reduces to the parallel (isostrain) model of rule of mixture [eq. (3), upper bound], and as $\zeta \to 0$, eq. (1) reduces to the series (isostress) model of rule of mixture [eq. (4), lower bound].[34]

$$E_c = \varphi_f E_f + (1 - \varphi_f) E_m \tag{3}$$

$$\frac{1}{E_c} = \frac{\varphi_f}{E_f \varphi_f} + \frac{(1 - \varphi_f)}{E_m} \tag{4}$$

The values of E_m and E_f used in the calculations were 1.13 GPa for the Nylon 6 matrix (Table III) and 200 GPa for a silicate-lamella.[35] The solid lines marked P and S indicate the upper and lower bounds calculated using the parallel and series model proposed by Halpin-Tsai.[34,36] In Figure 10, the modulus of NCE1 was above the P-curve, and the other NCHs also predict the aspect ratio to be approximately 200∼400. However, the aspect ratio observed from the TEM photographs was about 150. The deviations between the calculation and the experiment might come from the crystallinity of nylon 6 and the interaction bonding between the silicate lamella and nylon 6. Incorporating silicate into nylon 6 could dramatically increase the crystallization rate and the crystallinity. The higher crystallinity of the NCHs matrix leads to higher modulus than that of the neat nylon 6. The perfect crystalline would make the nylon 6 chain orientation more ordered and also lead to the higher modulus. Furthermore, the two intercalated modifiers provide more hydrogen bonding interaction and strongly enhance the mechanic properties of NCHs. Because of the higher crystallinity, the ordering orientation and the excellent interaction, the experiment data have higher modulus than the theoretical calculation.

The notched Izod impact strength was summarized in Table III. We found that the impact strength of NCHs were lower than the pristine NY6. This phenomenon was also mention in previous study[17] due to the lower fracture energy of lower molecular weight nylon 6. Because of higher crystallinity of NCE series, they showed dramatically decrease in impact strength. In contrast, the NCA series exhibited higher toughness than the ones of NCE due to the less crystalline modifier. This result showed consistent behavior as the tensile test.

The permeation properties were evaluated by measuring the water vapor permeation rate (WVPR) of each NCHs, as shown in Figure 11. The WVPR of NCHs was about 25% that of the neat nylon 6. The mechanism of the improvement on gas barrier properties is suggested to involve an increase in the tortuosity of the diffusive path of a penetrating molecule. Therefore, gas diffusion could be significantly affected by the morphology of the samples. As mentioned above, the NCE samples had a

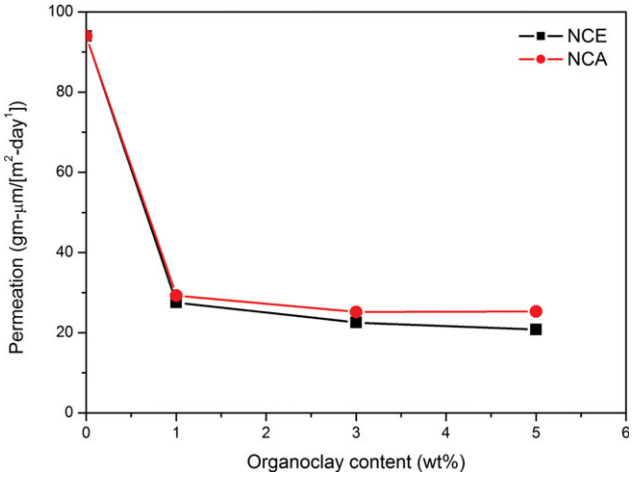

Figure 11. Water vapor permeation rate of NCHs. [Color figure can be viewed in the online issue, which is available at wileyonlinelibrary.com.]

higher crystallinity than the NCA ones, causing the NCE samples to have a lower WVPR.

CONCLUSIONS

The fully exfoliated NCHs nanocomposites in low molecular weight were successfully made by the modified masterbatch with wet kneading and introducing alkylamide and polyamide as modifiers, using the melt compounding process. Prior to melt compounding process, the wet kneading process provided higher shear force to make the swollen organoclay delaminate. Incorporation of the amide modifiers, the NCHs not only increased the crystallization rate but also showed the more perfect α form morphology. The mechanical properties of the NCHs could be strongly enhanced. Furthermore, the tensile fracture of NCHs reveals perfect cone-like patterns, which have been attributed to extensive plastic fibrillation of the nylon 6 matrix, assisted by the stress concentration and the strengthened effect caused by the silicate platelets in the well-exfoliated nanocomposites. The WVPR of NCHs was about 25% that of neat nylon 6.

ACKNOWLEDGMENTS

The financial support of the National Science Council of the Republic of China (NSC 99-2221-E-006-252, NSC 100-3113-E-024-001-CC2, NSC 100-2221-E-006-056-MY3 and NSC 100-2622-E-006-029-CC2) is gratefully acknowledged.

REFERENCES

1. Usuki, A.; Kojima, Y.; Kawasumi, M.; Okada, A.; Fukushima, Y.; Kurauchi, T.; Kamigaito, O. *J. Mater. Res.* **1993,** *8*, 1179.
2. Kojima, Y.; Usuki, A.; Kawasumi, M.; Okada, A.; Kurauchi, T.; Kamigaito, O. *J. Polym. Sci. Part A: Polym. Chem.* **1993,** *31*, 983.
3. Fornes, T. D.; Paul, D. R. *Polymer* **2003,** *44*, 4993.
4. Vaia, R. A.; Price, G.; Ruth, P. N.; Nguyen, H. T.; Lichtenhan, J. *Appl. Clay Sci.* **1999,** *15*, 67.
5. Giannelis, E. P. *Adv. Mater.* **1996,** *8*, 29.
6. Giannelis, E. P. *Appl. Organometal. Chem.* **1998,** *12*, 675.
7. Xie, S.; Zhang, S.; Wang, F.; Liu, H.; Yang, M. *Polym. Eng. Sci.* **2005,** *45*, 1247.
8. Kashiwagi, T.; Harris, R. H.; Zhang, X.; Briber, R. M.; Cipriano, B. H.; Raghavan, S. R.; Awad, W. H.; Shields, J. R. *Polymer* **2004,** *45*, 881.
9. Shanmuganathan, K.; Deodhar, S.; Dembsey, N.; Fan, Q.; Calvert, P. D.; Warner, S. B.; Patra, P. K. *J. Appl. Polym. Sci.* **2007,** *104*, 1540.
10. Thellen, C.; Schirmer, S.; Ratto, J. A.; Finnigan, B.; Schmidt, D. *J. Membr. Sci.* **2009,** *340*, 45.
11. Tsai, Y.; Fan, C.-H.; Hung, C.-Y.; Tsai, F.-J. *Polym. Compos.* **2011,** *32*, 89.
12. Vaia, R. A.; Ishii, H.; Giannelis, E. P. *Chem. Mater.* **1993,** *5*, 1694.
13. Vaia, R. A.; Jandt, K. D.; Kramer, E. J.; Giannelis, E. P. *Macromolecules* **1995,** *28*, 8080.
14. Liu, L.; Qi, Z.; Zhu, X. *J. Appl. Polym. Sci.* **1999,** *71*, 1133.
15. Cho, J. W.; Paul, D. R. *Polymer* **2001,** *42*, 1083.
16. Dennis, H. R.; Hunter, D. L.; Chang, D.; Kim, S.; White, J. L.; Cho, J. W.; Paul, D. R. *Polymer* **2001,** *42*, 9513.
17. Fornes, T. D.; Yoon, P. J.; Keskkula, H.; Paul, D. R. *Polymer* **2001,** *42*, 09929.
18. Fornes, T. D.; Yoon, P. J.; Hunter, D. L.; Keskkula, H.; Paul, D. R. *Polymer* **2002,** *43*, 5915.
19. Yoon, P. J.; Fornes, T. D.; Paul, D. R. *Polymer* **2002,** *43*, 6727.
20. Fornes, T. D.; Paul, D. R. *Polymer* **2003,** *44*, 3945.
21. Fornes, T. D.; Hunter, D. L.; Paul, D. R. *Macromolecules* **2004,** *37*, 1793.
22. Shah, R. K.; Paul, D. R. *Polymer* **2004,** *45*, 2991.
23. Hasegawa, N.; Okamoto, H.; Kato, M.; Usuki, A.; Sato, N. *Polymer* **2003,** *44*, 2933.
24. Okada, A.; Usuki, A. *Mater. Sci. Engi. C* **1995,** *3*, 109.
25. Usuki, A.; Kawasumi, M.; Kojima, Y.; Okada, A.; Kurauchi, T.; Kamigaito, O. *J. Mater. Res.* **1993,** *8*, 1174.
26. L. Shen, W. C. Tjiu, T. Liu, *Polymer* **2005,** *46*, 11969.
27. Li, Y.; Shimizu, H. *J. Polym. Sci. Part B: Polym. Phys.* **2006,** *44*, 284.
28. Miri, V.; Elkoun, S.; Peurton, F.; Vanmansart, C.; Lefebvre, J. M.; Krawczak, P.; Seguela, R. *Macromolecules* **2008,** *41*, 9234.
29. Kim, G.-M.; Goerlitz, S.; Michler, G. H. *J. Appl. Polym. Sci.* **2007,** *105*, 38.
30. Li, T.-C.; Ma, J.; Wang, M.; Tjiu, W. C.; Liu, T.; Huang, W. *J. Appl. Polym. Sci.* **2007,** *103*, 1191.
31. Uribe-Arocha, P.; Mehler, C.; Puskas, J. E.; Altstädt, V. *Polymer* **2003,** *44*, 2441.
32. Xie, S.; Zhang, S.; Zhao, B.; Qin, H.; Wang, F.; Yang, M. *Polym. Int.* **2005,** *54*, 1673.
33. Xie, S.; Zhang, S.; Wang, F.; Yang, M.; Séguéla, R.; Lefebvre, J.-M. *Compos. Sci. Technol.* **2007,** *67*, 2334.
34. Wilkinson, A. N.; Man, Z.; Stanford, J. L.; Matikainen, P.; Clemens, M. L.; Lees, G. C.; Liauw, C. M. *Compos. Sci. Technol.* **2007,** *67*, 3360.
35. Chen, B.; Evans, J. R. G. *Scripta Materialia* **2006,** *54*, 1581.
36. Affdl, J. C. H.; Kardos, J. L. *Polym. Eng. Sci.* **1976,** *16*, 344.